Spin-dependent $\pi\pi^*$ gap in graphene on a magnetic substrate

https://dx.doi.org/10.1103/PhysRevLett.132.266401

P. M. Sheverdyaeva,[1,*] G.Bihlmayer,[2] E. Cappelluti,[1] D. Pacilé,[3] F. Mazzola,[4] N. Atodiresei,[5] M. Jugovac,[6] I. Grimaldi,[3] G. Contini,[7] A. K. Kundu[†],[1,8] I. Vobornik,[9] J. Fujii,[9] P. Moras,[1] C. Carbone,[1] and L. Ferrari[9,‡]

[1]*CNR-Istituto di Struttura della Materia (CNR-ISM), Strada Statale 14, km 163.5, 34149 Trieste (Italy)*
[2]*Peter Grünberg Institut and Institute for Advanced Simulation, Forschungszentrum Jülich and JARA, 52425 Jülich, Germany*
[3]*Dipartimento di Fisica, Università della Calabria, 87036 Arcavacata di Rende (CS), Italy*
[4]*Istituto Officina dei Materiali (IOM)-CNR, Laboratorio TASC, Strada Statale 14 km 163.5, 34149, Trieste, Italy*
[5]*Peter Grünberg Institut and Institute for Advanced Simulation, Forschungszentrum Jülich and JARA, 52425 Jülich, Germany*
[6]*Elettra Sincrotrone Trieste, Strada Statale 14 km 163.5, 34149 Trieste, Italy*
[7]*CNR-Istituto di Struttura della Materia (CNR-ISM), Via del Fosso del Cavaliere 100, 00133 Roma (Italy)*
[8]*International Center for Theoretical Physics (ICTP), Trieste, 34151, Italy*
[9]*CNR-Istituto Officina dei Materiali (CNR-IOM), S.S. 14, km 163.5, 34149 Trieste (Italy)*

(Dated: October 18, 2024)

We present a detailed analysis of the electronic properties of graphene/Eu/Ni(111). By using angle and spin-resolved photoemission spectroscopy and ab initio calculations, we show that the intercalation of Eu in the graphene/Ni(111) interface gives rise to a gapped freestanding dispersion of the $\pi\pi^*$ Dirac cones at the $\bar{\mathrm{K}}$ point with an additional lifting of the spin degeneracy due to the mixing of graphene and Eu states. The interaction with the magnetic substrate results in a large spin-dependent gap in the Dirac cones with a topological nature characterized by a large Berry curvature, and a spin-polarized van Hove singularity, whose closeness to the Fermi level gives rise to a polaronic band.

Graphene is a highly promising material for spintronics applications due to its large spin transport coherence length [1, 2], and its particular band structure, especially for the massless Dirac cones and the nearly flat van Hove singularities (VHSs) [3–7]. Despite graphene being a non-magnetic material, it can acquire spin polarization by the proximity effect in contact with magnetic materials. However, on transition metals Fe, Co, and Ni the interaction with $3d$ states strongly modifies the $\pi\pi^*$ states, which form complex hybrid bands and lose their linear character [8–11]. One of the goals of spintronics would be turning graphene into a spin-conductor, finding supporting magnetic materials that preserve the graphene electronic properties almost unaltered [5–7, 12]. Removing the spin degeneracy may turn graphene into a spin field effect transistor [13], spin valve [14], or spin-transfer torque device [15]. In turn, a spin-polarized VHS may lead to unconventional superconductivity [16], quantum phases[17], and insulating topological states [18, 19].

Recent works have addressed the intercalation in graphene/ferromagnet heterostructures [9, 19–27], where the π and π^* bands recover their characteristic linearity. In particular, the rare earth metallic intercalants additionally induce a heavy electron doping that brings the VHS to the proximity of the Fermi level (FL) [19–21]. A remarkable example is the Eu intercalated graphene/Ni(111) system, which has been studied by density functional theory (DFT) calculations and x-ray magnetic circular dichroism (XMCD) [21]. The calculations show that the $2p$ states of C atoms lose the characteristic hybridization with the $3d$ states of Ni. The electron density of states (DOS) is spin-dependent and the XMCD data show that the Eu monolayer (ML) is ferromagnetic within the layer while being antiferromagnetically coupled to the Ni underlayer. The presence of the Ni film leads to a magnetic ordering above room temperature in the Eu layer, in contrast to the case of an iridium substrate that leads to a much lower transition temperature [28]. This makes the graphene/Eu/Ni(111) system interesting for possible applications in spintronics.

In this Letter, we investigate the electronic and magnetic properties of graphene/Eu/Ni(111), carried out by angle- and spin-resolved photoemission spectroscopy (ARPES and spin-ARPES), and DFT calculations. Our results show that, as a consequence of the intercalation, graphene is decoupled from Ni, and its $\pi\pi^*$ states recover a linear dispersion in the proximity of the $\bar{\mathrm{K}}$ point. The interaction with the Eu $4f$ states removes the spin degeneracy near the Dirac point and induces a large spin-dependent gap between the π and π^* bands. The large Eu-induced n-doping leads to the emergence of a spin-polarized VHS at FL and a pronounced quasiparticle band. In the vicinity of the energy gap, our calculations suggest the presence of a large Berry curvature, corroborating the

[†]Present address: Condensed Matter Physics and Materials Science Division, Brookhaven Nat Lab, Upton, NY 11973, USA
[*]Electronic address: polina.sheverdyaeva@ism.cnr.it
[‡]Electronic address: luisa.ferrari@ism.cnr.it

topological nature of the bands [29, 30].

Fig. 1(a) shows the calculated band structure of graphene/Eu/Ni(111) (for details see Sec. I of Supplemental Material (SM)[31]). The system forms a $(\sqrt{3}\times\sqrt{3})$ $R30°$ superstructure with respect to the pristine graphene and Ni(111) lattices [21]. Its bands are folded as indicated in Fig. 1(b) and by the x-axis labels of Fig. 1(a). Since the superlattice-related replicas are not experimentally observed in our photoemission study, due to a weakening of the scattering potential after the intercalation [11, 19, 53], we will not consider the folding-induced bands and will refer to the (1×1) surface for the indexing. The graphene's $\pi\pi^*$ bands are shifted to higher binding energy with respect to freestanding graphene (see Fig. S1(a) of SM Sec. I[31]), due to the electron doping from Eu. The position of the Dirac cone overlaps with the Eu $4f$ minority states shown by green color (Fig. 1). The magnitude of the doping-induced shift (1.4 eV approximately) is similar to the one observed in other graphene systems doped with rare earth or alkaline metals [4, 54–57].

Figs. 1(c) and 1(d) show a zoom of the region of the Dirac point along $\bar{\Gamma}\bar{\mathrm{K}}$ (k_y) and the perpendicular direction, p($\bar{\Gamma}\bar{\mathrm{K}}$) ($k_x$), respectively, indicated in the Fig. 1(b), revealing several important details in the graphene band structure. First, the $\pi\pi^*$ bands exhibit close to $\bar{\mathrm{K}}$ a conical dispersion, typical of a gapped quasi-freestanding graphene [9, 58, 59], indicating that the Eu intercalation attenuates the graphene-Ni interaction. Second, the graphene states acquire a spin-polarization in some defined binding energy and wave vector regions where they interact with the Eu states. A large gap of about 900 meV opens for the spin-minority channel, mostly due to the hybridization with the polarized Eu $4f$ states (see SM Sec. I[31]). For the majority-spin states, which are not affected by the interaction with the Eu $4f$, the gap is about 150 meV. Furthermore, we notice in the $\bar{\Gamma}\bar{\mathrm{K}}$ direction a strong bending of the Dirac π^* band (Fig. 1(a)). Such flat dispersion is related to the presence of the VHS at the $\bar{\mathrm{M}}$ point, which is shifted close to FL because of the large electron doping (Fig. S1(a,b) of SM Sec. I[31]). The interaction with the spin-polarized Eu sp-bands is expected to induce a spin polarization also for the π^* bands associated with the VHS. This is clearly seen in Fig. S1(b) of SM[31], which shows the calculated band structures of graphene on Eu without the Ni substrate, where the VHS shows two spin-split branches. On a Ni substrate, the indirect interaction with Ni states leads to a stronger delocalization of the VHS's minority spin branch, so only the majority branch can be observed (see Fig. S2(a,b) of SM Sec. I[31] for the corresponding densities of states). Similar results on the VHS properties were recently reported for the graphene/Eu/Co(0001) [19].

ARPES and spin-ARPES measurements were performed in order to confirm the dispersion and spin-polarization of the graphene $\pi\pi^*$ bands, in particular near the Dirac point, predicted by the theoretical calculations (for details see Sec. II of SM[31]). Figs. 2(a) and 2(b) show the ARPES data of the system close to $\bar{\mathrm{K}}$ along k_y and k_x, respectively, that can be compared to Figs. 1(c) and 1(d). Dispersing graphene bands are crossed by a broad flat Eu $4f$ state close to 1.5 eV. We can confirm the effects of doping and an almost linear dispersion of the $\pi\pi^*$ bands (see also Fig. S4 of SM Sec. II[31]). The second derivative spectra more clearly indicate the presence of two cone-like features and the opening of two different energy gaps at the $\bar{\mathrm{K}}$ point (Figs. 2(c,d)), that amount to 250 ± 50 meV (blue arrows) and 1100 ± 50 meV (red arrows). Fig. 2(e) reports the spin-integrated energy distribution curves (EDCs) extracted from the p($\bar{\Gamma}\bar{\mathrm{K}}$) map, where it is possible to follow the dispersion of the $\pi\pi^*$ states for the two spin channels. These results are in agreement with the DFT predictions for two spin-dependent gaps, that we further confirm by spin-ARPES measurements. We analyzed the spin polarization at two different wave vectors: away from the Dirac point, where only the Eu $4f$ states are visible ($k_x = -0.8$ Å^{-1}), and at the Dirac point ($k_x = 0$ Å^{-1}), where Eu and graphene states overlap (black dashed lines in Fig. 2(b)). Figs. 2(f-i) show the corresponding majority and minority intensities (panels (f,h)) and spin polarization curves (panels (g,i)). Away from the $\bar{\mathrm{K}}$ point, we confirm the spin polarization of the Eu $4f$ states: the majority- and minority- states of Eu (at $\sim$ 1.5 eV) show two similar large single-peak energy profiles with a non-complete spin polarization of about 15%, due to the finite temperature and a non-complete magnetic saturation of the sample (Figs. 2(f,g)). The sharp peaks just below FL are the Ni states with prevalent polarization opposite to the Eu $4f$ states. At the $\bar{\mathrm{K}}$ point, the majority- and minority-spin states show two-peaked profiles with clearly different energy distances between the peaks (Fig. 2(h)). We can distinguish the corresponding minima and maxima in the spin polarization spectra (Fig. 2(i)), better visible for π states, and estimate the peak separation to be about (400 ± 100) meV for the majority-spin channel and (1050 ± 100) meV for the minority-spin channel. These results are in agreement with the majority and minority gap values provided by our calculations.

Close to FL we can notice in Figs. 2(a,c) a strong bending of the π^* band with increasing the k_y values (towards the $\bar{\mathrm{M}}$ point). Such feature is in a very good agreement with the DFT calculations that predict the VHS of the π^* band to be located just above FL [4, 19, 60]. Figs. 3(a) and 3(b) show the experimental Fermi surface where the VHS is marked by black arrows. In the ARPES maps (Figs. 3(c,d)) it can be observed as a weak intensity right at FL that extends towards the $\bar{\mathrm{M}}$ point. Due to the low intensity of the VHS, we were not able to access experimentally its spin polarization. The agreement between the DFT calculations and our ARPES and spin-ARPES data for the Dirac cone suggests that the VHS preserves a spin-polarization with minority character, similarly to the graphene/Eu/Co system[19].

In Figs. 2(a-e) we can also notice a second low-dispersive feature, which stems out from the Dirac cone at about

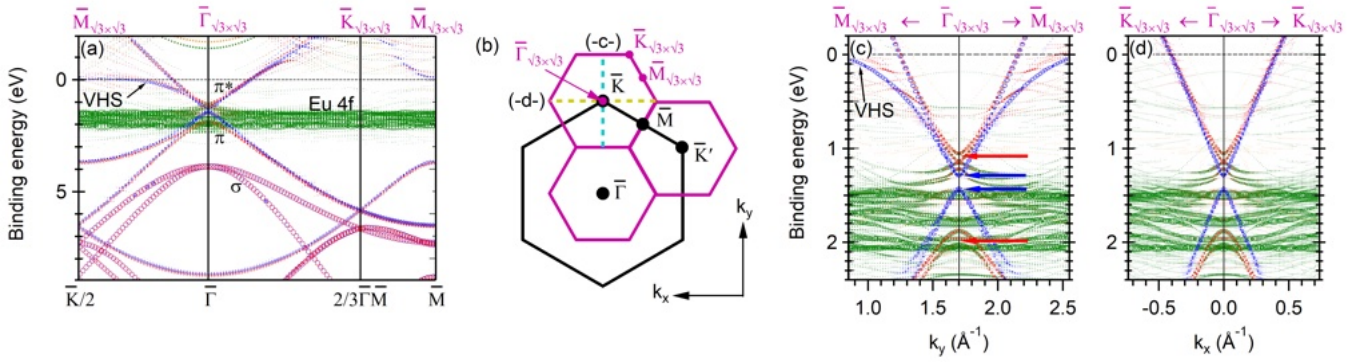

Figure 1: (a) Spin resolved DFT band structure calculated for graphene/Eu/Ni/(111) along the main high symmetry directions. The red (blue) color indicates the graphene minority (majority) bands. The green (yellow) color indicates the Eu minority (majority) spin channels. The weight of the Ni states, in the background, is artificially reduced for clarity. (b) Schematic of the surface BZs of the (1×1) graphene/Ni(111) (black), and the $(\sqrt{3} \times \sqrt{3})$ $R30^\circ$ superstructure (magenta). The two segments, investigated by theory and experiment, are drawn in yellow and light blue colors. (c) and (d) Zoom of the calculated bands along $\bar{\Gamma}\bar{K}$ and p($\bar{\Gamma}\bar{K}$), respectively. Red (blue) arrows indicate the minority (majority) cones. The binding energy scale is referred to FL.

.

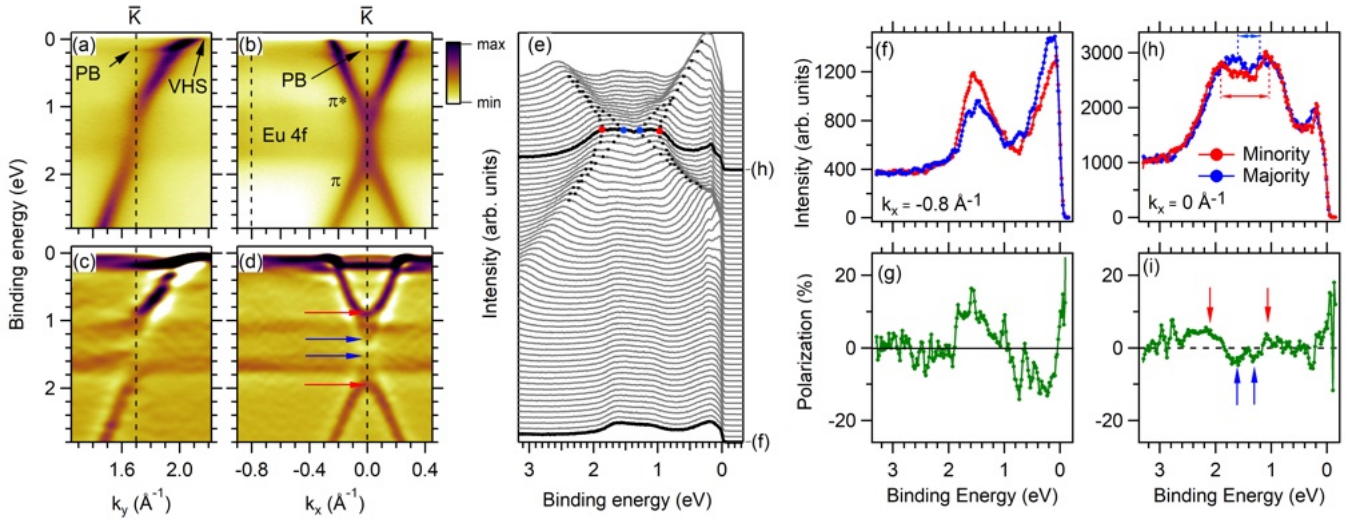

Figure 2: (a-d) Spin-integrated ARPES maps of graphene/Eu/Ni(111) (a,c) along the $\bar{\Gamma}\bar{K}$ direction and (b,d) along the p($\bar{\Gamma}\bar{K}$) directions. (a,b) As-taken data and (c,d) their second derivative along the energy axis. (e) EDC spectra extracted from the map shown in panel (b). Black dots follow the dispersion of the π and π^* states for the two spin channels. The bolded lines correspond to $k_x = 0$ and $k_x = -0.8$ Å^{-1}. Red (blue) dots indicate the edges of the minority (majority) gap. The non-dispersive peak at 180 meV of binding energy is the PB band. (f,h) Minority-spin (red curves) and majority-spin (blue curves) EDCs at (f) $k_x = -0.8$ Å^{-1} and (h) $k_x = 0$ Å^{-1} (as the dashed lines indicate in (b)). Red (blue) arrows indicate the width of the minority (majority) gap. (g,i) Spin polarizations corresponding to the spectra shown in panels (f,h), respectively. Data were acquired at 25 K and a photon energy of 50 eV.

180 meV of binding energy. We identify the nature of this spectral feature as related to polaronic effects, and we denote it as polaronic band (PB). Such spectral feature, which is also clearly visible in Figs. 3(c-f), is absent in the DFT simulations. We can observe that it extends towards $\bar{M}$ as a replica of the VHS in Fig. 3(c). A kink at a similar binding energy is commonly observed in graphene bands and is attributed to electron-phonon (el-ph) coupling [58, 61–63]. While a band similar to PB is observed on highly n-doped graphenes close to $\bar{M}$, it is rarely reported at $\bar{K}$ [4, 19, 56, 64, 65], and often attributed to the substrate or dopants [19, 64, 65]. This hypothesis is in contrast with the variety of systems where this band was observed. The 180 meV binding energy corresponds to the phonon mode of graphene, and indeed several studies associated the PB band to a strong el-ph coupling in the polaronic regime [4, 56], boosted by the closeness of the VHS. Our findings support this view: in Fig. 3(d)

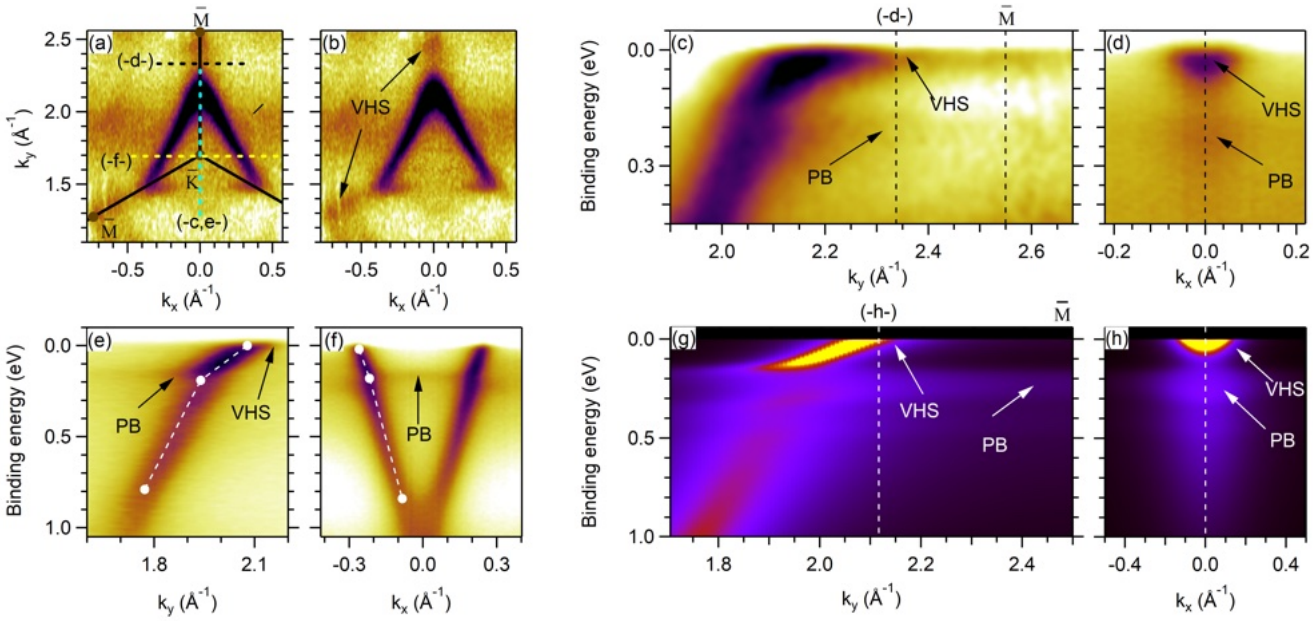

Figure 3: (a,b) Experimental Fermi surface of graphene/Eu/Ni(111) with and without the surface Brillouin zone on top (hν=50 eV). (c) ARPES maps along $\bar{\Gamma}\bar{M}$ with an enhanced contrast (hν=40 eV). (d) Cut perpendicular to $\bar{\Gamma}\bar{K}$ direction at the point indicated by the black dashed line in (a) and (c) (hν=75 eV); (e,f) ARPES spectra along $\bar{\Gamma}\bar{K}$ and p($\bar{\Gamma}\bar{K}$) showing the zoom on the vicinity of PB band, white dashed lines indicate the slope of the π^* band in the proximity of the kink (hν=50 eV); (g,h) Theoretical simulations of the ARPES spectral function along the same cuts as in panels (c)-(d) including the many-body effects of the retarded electron-phonon self-energy. The binding energy scale is referred to FL.

the main spectral feature at low-energy $\omega \approx 0$ associated with the VHS, is accompanied by a weak replica at $\omega \approx 160 - 180$ meV, where no DFT bands are expected, with the typical profile of a polaronic replica [56, 66] (see Fig. S5 of SM Sec. III[31]). We confirm the robustness of this interpretation by performing many-body self-consistent calculations of the retarded el-ph self-energy in the strong-coupling regime (see Sec. III of SM[31] for details). From the ratio of the low-energy and high-energy slopes (see Figs. 3(e,f)) we estimate $\lambda = 1.63$ and $\lambda = 0.3$ along $\bar{\Gamma}\bar{K}$) and $p(\bar{\Gamma}\bar{K})$, respectively. The resulting spectral features along $\bar{\Gamma}\bar{K}$ and $p(\bar{\Gamma}\bar{K})$, are shown in Figs. 3(g,h). The so-extended observed polaronic band is well reproduced when the VHS is placed in the proximity of FL. The result of the model, using the same strength of el-ph coupling but with the VHS far from FL, leads to a much weaker PB band (see Fig. S6 and Sec. III of SM [31]). This demonstrates a direct relation of PB to the VHS band at FL and hence to the large n-doping induced by Eu.

The above reported large and spin-dependent graphene's gap can give rise to a number of effects for spintronic applications, such as spin-filtering, spin-selective injections or the quantum anomalous Hall effect. Regarding the latter, we evaluated the topological character of the gap by calculating the Berry curvature [67, 68] of a $(\sqrt{3}\times\sqrt{3})R30°$ Eu in contact with freestanding graphene (see Fig. S1(b) of SM Sec. I[31]). Fig. 4(a) shows the Berry curvature $\Omega^z{}_n$ [69] as a function of binding energy and wave vector in the proximity of the Dirac cone, for the in-plane spin polarization, corresponding to the present experimental case. We can observe a finite Berry curvature that gives rise to a sizeable k-resolved integral curvature (Fig. 4(b)). Higher values can be obtained for the out-of-plane spin polarization direction (Figs. 4(c,d)) that can be experimentally realized, for example, on a thin Co substrate [70]. Due to the $(\sqrt{3}\times\sqrt{3})R30°$ reconstruction, there is an overlap of the Dirac cone with the Eu sp-states, and a superposition of two opposite contributions from $\bar{K}$ and $\bar{K}'$ leading to a lowering of the integral curvature. In order to cross-check our findings, we also analyzed the (2×2) graphene/Eu system (Fig. S7(a) of SM Sec. IV[31]), that can be realized on Ir(111) [28]. The disentanglement of the contributions from $\bar{K}$, $\bar{K}'$ and Eu sp-band provides a simpler electronic pattern in the proximity of the Dirac point, and leads to an increase of the Berry curvature values by orders of magnitude (Figs. S7(b,c) of SM Sec. IV[31]). For this system, we also calculated the anomalous Hall conductivity and found that it reaches about $-e^2/h$ at the minority gap (Fig. S8 of SM Sec. IV[31], red arrows). This finding, according to the literature [68, 71, 72], elucidates the possibility of turning the graphene-Eu heterostructures into candidate systems for quantum anomalous Hall effect. In conclusion, through theoretical studies and experimental evidence, we show that graphene on a magnetic Eu presents an almost unaltered dispersion of the $\pi\pi^*$ states together with a lifting of spin degeneracy and a large electron doping. DFT predicts that, at the Dirac point,

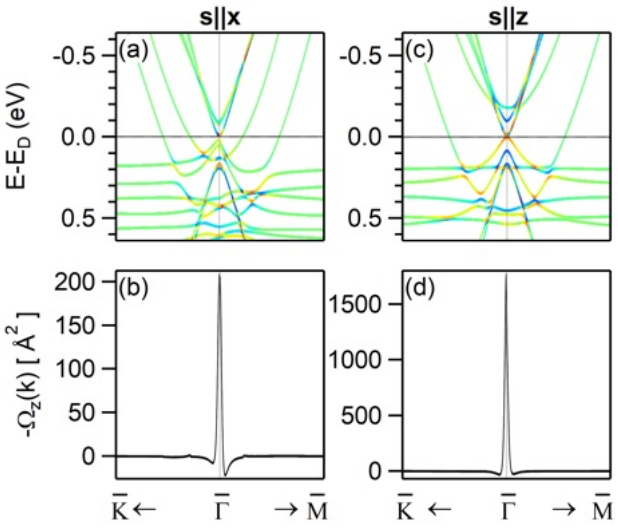

Figure 4: Berry curvature calculation. (a) k-resolved Berry curvature for the graphene/Eu system with in-plane spin direction in the proximity of the Dirac cone along the $\bar{K}\bar{\Gamma}\bar{M}$ direction. The energy scale is referred to the Dirac point. The color scale is logarithmic where red=positive, green=zero, blue=negative. (b) Band-integrated k-resolved Berry curvature, taken on the valence states. (c,d) same as (a,b) for an out of plane spin direction.

a large energy gap opens for the minority spin channel due to the spin-dependent interaction with Eu 4f states, while in the opposite spin channel, which is undisturbed by substrate states, a smaller gap opens. ARPES and spin-ARPES data provide experimental evidence for this spin-polarized gap. We furthermore report on the spectroscopic signature of a polaronic band and demonstrate its direct relation to the large Eu-induced n-doping and the VHS. A finite Berry curvature across the gap and the breaking of the time-reversal symmetry allow for the emergence of a quantum anomalous Hall effect in this system.

Acknowledgements

G.B. and N.A. gratefully acknowledge the computing time granted by the JARA Vergabegremium and provided on the JARA Partition part of the supercomputer JURECA at Forschungszentrum Jülich. N.A. acknowledges DFG support within CRC1238, project no. 277146874-CRC 1238 (subproject C01)". E.C. acknowledges financial support from PNRR MUR Project No. PE0000023-NQSTI. A.K.K. received funding from the US Department of Energy, Office of Basic Energy Sciences, contract no. DE-SC0012704. Authors acknowledge Elettra Sincrotrone Trieste for providing access to its synchrotron radiation facilities and for financial support under the SUI internal project and EUROFEL-ROADMAP ESFRI of the Italian Ministry of University and Research. This work has been partly performed in the framework of the nanoscience foundry and fine analysis (NFFA-MUR Italy Progetti Internazionali) facility.

[1] N. Tombros, C. Jozsa, M. Popinciuc, H. T. Jonkman, and B. J. Van Wees, Nature **448**, 571 (2007).
[2] T. Maassen, J. J. Van Den Berg, N. Ijbema, F. Fromm, T. Seyller, R. Yakimova, and B. J. Van Wees, Nano Letters **12**, 1498 (2012).
[3] L. Van Hove, Phys. Rev. **89**, 1189 (1953).
[4] J. L. McChesney, A. Bostwick, T. Ohta, T. Seyller, K. Horn, J. González, and E. Rotenberg, Physical Review Letters **104**, 136803 (2010).
[5] K. S. Novoselov, A. K. Geim, S. V. Morozov, D. Jiang, M. I. Katsnelson, I. V. Grigorieva, S. V. Dubonos, and A. A. Firsov, Nature **438**, 197 (2005).
[6] A. K. Geim and K. S. Novoselov, Nature Materials **6**, 183 (2007).
[7] A. H. Castro Neto, F. Guinea, N. M. R. Peres, K. S. Novoselov, and A. K. Geim, Reviews of Modern Physics **81**, 109 (2009).
[8] D. Pacilé, S. Lisi, I. Di Bernardo, M. Papagno, L. Ferrari, M. Pisarra, M. Caputo, S. K. Mahatha, P. M. Sheverdyaeva, P. Moras, P. Lacovig, S. Lizzit, A. Baraldi, M. G. Betti, and C. Carbone, Phys. Rev. B **90**, 195446 (2014).
[9] A. Varykhalov, J. Sánchez-Barriga, A. M. Shikin, C. Biswas, E. Vescovo, A. Rybkin, D. Marchenko, and O. Rader, Physical Review Letters **101**, 157601 (2008).
[10] A. Varykhalov and O. Rader, Phys. Rev. B **80**, 035437 (2009).
[11] M. Jugovac, C. Tresca, I. Cojocariu, G. Di Santo, W. Zhao, L. Petaccia, P. Moras, G. Profeta, and F. Bisti, Phys. Rev. B **105**, L241107 (2022).
[12] K. S. Novoselov, V. I. Fal'Ko, L. Colombo, P. R. Gellert, M. G. Schwab, and K. Kim, Nature **490**, 192 (2012).
[13] Y. G. Semenov, K. W. Kim, and J. M. Zavada, Applied Physics Letters **91**, 153105 (2007).
[14] E. W. Hill, F. Schedin, and P. Blake, IEEE Transactions on Magnetics **42**, 2694 – 2696 (2006).
[15] B. Zhou, X. Chen, H. Wang, K.-H. Ding, and G. Zhou, Journal of Physics Condensed Matter **22**, 445302 (2010).
[16] Z. Liu, F. Liu, and Y.-S. Wu, Chinese Physics B **23**, 077308 (2014).
[17] K. Sun, Z. Gu, H. Katsura, and S. Das Sarma, Phys. Rev. Lett. **106**, 236803 (2011).
[18] M. Kang, S. Fang, L. Ye, H. C. Po, J. Denlinger, C. Jozwiak, A. Bostwick, E. Rotenberg, E. Kaxiras, J. G. Checkelsky, and R. Comin, Nature Communications **11**, 4004 (2020).
[19] M. Jugovac, I. Cojocariu, J. Sánchez-Barriga, P. Gargiani, M. Valvidares, V. Feyer, S. Blügel, G. Bihlmayer, and P. Perna, Advanced Materials **35**, 2301441 (2023).
[20] E. N. Voloshina and Y. S. Dedkov, Zeitschrift fur Natur-

forschung - Section A Journal of Physical Sciences **69**, 297 (2014).
[21] F. Huttmann, D. Klar, N. Atodiresei, C. Schmitz-Antoniak, A. Smekhova, A. J.Martínez-Galera, V. Caciuc, G. Bihlmayer, S. Blügel, T. Michely, and H. Wende, Physical Review B **95**, 075427 (2017).
[22] M. Weser, E. Voloshina, K. Horn, and Y. S. Dedkov, Physical Chemistry Chemical Physics **13**, 7534 (2011).
[23] E. Voloshina, A. Generalov, M. Weser, S. Böttcher, K. Horn, and Y. S. Dedkov, New Journal of Physics **13**, 113028 (2011).
[24] A. Grüneis and D. V. Vyalikh, Physical Review B **77**, 193401 (2008).
[25] O. Vilkov, A. Fedorov, D. Usachov, L. Yashina, A. Generalov, K. Borygina, N. Verbitskiy, A. Grüneis, and D. Vyalikh, Scientific Reports **3**, 2168 (2013).
[26] Y. S. Park, J. H. Park, H. N. Hwang, T. S. Laishram, K. S. Kim, M. H. Kang, and C. C. Hwang, Phys. Rev. X **4**, 031016 (2014).
[27] Y. Dedkov, W. Klesse, A. Becker, F. Spaeth, C. Papp, and E. Voloshina, Carbon **121**, 10 (2017).
[28] S. Schumacher, F. Huttmann, M. Petrović, C. Witt, D. F. Förster, C. Vo-Van, J. Coraux, A. J. Martínez-Galera, V. Sessi, I. Vergara, R. Rückamp, M. Grüninger, N. Schleheck, F. Meyer Zu Heringdorf, P. Ohresser, M. Kralj, T. O. Wehling, and T. Michely, Physical Review B - Condensed Matter and Materials Physics **90**, 235437 (2014).
[29] C. L. Kane and E. J. Mele, Phys. Rev. Lett. **95**, 226801 (2005).
[30] N. Fläschner, B. S. Rem, M. Tarnowski, D. Vogel, D.-S. Lühmann, K. Sengstock, and C. Weitenberg, Science **352**, 1091 (2016).
[31] See Supplemental Material at XXX, which includes Refs. [32–52], for additional information about the experimental methods and a detailed discussion of the numerical simulations.
[32] J. P. Perdew, K. Burke, and M. Ernzerhof, Physical Review Letters **77**, 3865 (1996).
[33] K. Lee, E. D. Murray, L. Kong, B. I. Lundqvist, and D. C. Langreth, Phys. Rev. B **82**, 081101(R) (2010).
[34] A. D. Becke, The Journal of Chemical Physics **84**, 4524 (1986).
[35] I. Hamada, Phys. Rev. B **89**, 121103(R) (2014).
[36] D. Wortmann, G. Michalicek, R. Hilgers, A. Neukirchen, H. Janssen, U. Grytsiuk, J. Broeder, and C.-R. Gerhorst, Fleur, 2023, 10.5281/zenodo.7778444.
[37] Y. Ren, X. Deng, Z. Qiao, C. Li, J. Jung, C. Zeng, Z. Zhang, and Q. Niu, Phys. Rev. B **91**, 245415 (2015).
[38] C. Chen, J. Avila, S. Wang, Y. Wang, M. Mucha-Kruczyński, C. Shen, R. Yang, B. Nosarzewski, T. P. Devereaux, G. Zhang, and M. C. Asensio, Nano Letters **18**, 1082 (2018).
[39] C. Chen, K. Nuckolls, S. Ding, W. Miao, D. Wong, M. Oh, R. Lee, S. He, C. Peng, D. Pei, Y. Li, S. Zhang, J. Liu, Z. Liu, C. Jozwiak, A. Bostwick, E. Rotenberg, C. Li, X. Han, D. Pan, X. Dai, C. Liu, B. Bernevig, Y. Wang, A. Yazdani, and Y. Chen, arXiv.:2303.14903 (2023).
[40] F. Marsiglio, M. Schossmann, and J. P. Carbotte, Phys. Rev. B **37**, 4965 (1988).
[41] G. M. Eliashberg, Sov. Phys. JETP **11**, 6966 (1960).
[42] G. Grimvall, *The electron-phonon interaction in metals*, North-Holland, Amsterdam, 1981.
[43] D. J. Scalapino, The Electron-Phonon Interaction and Strong-Coupling Superconductors, in *Superconductivity*, edited by R.D. Parks, page 449, Dekker, New York, 1969.
[44] A. Lanzara, P. Bogdanov, X. Zhou, S. Kellar, D. Feng, E. Lu, T. Yoshida, H. Eisaki, A. Fujimori, K. Kishio, J. Shimoyama, T. Noda, S. Uchida, Z. Hussain, and Z. Shen, Nature **412**, 510 (2001).
[45] F. Mazzola, J. W. Wells, R. Yakimova, S. Ulstrup, J. A. Miwa, R. Balog, M. Bianchi, M. Leandersson, J. Adell, P. Hofmann, and T. Balasubramanian, Phys. Rev. Lett. **111**, 216806 (2013).
[46] S. Engelsberg and J. R. Schrieffer, Phys. Rev. **131**, 993 (1963).
[47] E. Cappelluti, and L. Pietronero, Phys. Rev. B **68**, 224511 (2003).
[48] A. Knigavko, J. P. Carbotte, and F. Marsiglio, Europhysics Letters **71**, 776 (2005).
[49] G. D. Mahan, *Many Particle Physics*, Plenum, 2000.
[50] I. G. Lang, and Yu. A. Firsov, Sov. Phys. JETP **16**, 1301 (1963).
[51] S. Ciuchi, F. de Pasquale, S. Fratini, and D. Feinberg, Phys. Rev. B **56**, 4494 (1997).
[52] P. C. Pattnaik, C. L. Kane, D. M. Newns, and C. C. Tsuei, Phys. Rev. B **45**, 5714 (1992).
[53] I. I. Klimovskikh, M. M. Otrokov, V. Y. Voroshnin, D. Sostina, L. Petaccia, G. Di Santo, S. Thakur, E. V. Chulkov, and A. M. Shikin, ACS Nano **11**, 368 (2017).
[54] S. Sung, S. Kim, P. Lee, J. Kim, M. Ryu, H. Park, K. Kim, B. I. Min, and J. Chung, Nanotechnology **28**, 205201 (2017).
[55] L. Daukiya, M. N. Nair, S. Hajjar-Garreau, F. Vonau, D. Aubel, J. L. Bubendorff, M. Cranney, E. Denys, A. Florentin, G. Reiter, and L. Simon, Physical Review B **97**, 035309 (2018).
[56] S. Link, S. Forti, A. Stöhr, K. Küster, M. Rösner, D. Hirschmeier, C. Chen, J. Avila, M. C. Asensio, A. A. Zakharov, T. O. Wehling, A. I. Lichtenstein, M. I. Katsnelson, and U. Starke, Physical Review B **100**, 121407(R) (2019).
[57] P. Rosenzweig, H. Karakachian, S. Link, K. Küster, and U. Starke, Physical Review B **100**, 035445 (2019).
[58] M. Papagno, S. Rusponi, P. M. Sheverdyaeva, S. Vlaic, M. Etzkorn, D. Pacilé, P. Moras, C. Carbone, and H. Brune, ACS Nano **6**, 199 (2012).
[59] D. Pacilé, P. Leicht, M. Papagno, P. M. Sheverdyaeva, P. Moras, C. Carbone, K. Krausert, L. Zielke, M. Fonin, Y. S. Dedkov, F. Mittendorfer, J. Doppler, A. Garhofer, and J. Redinger, Physical Review B - Condensed Matter and Materials Physics **87**, 035420 (2013).
[60] N. Ehlen, M. Hell, G. Marini, E. H. Hasdeo, R. Saito, Y. Falke, M. O. Goerbig, G. Di Santo, L. Petaccia, G. Profeta, and A. Grüneis, ACS Nano **14**, 1055 (2020).
[61] A. Bostwick, T. Ohta, T. Seyller, K. Horn, and E. Rotenberg, Nature Physics **3**, 36 (2007).
[62] A. V. Fedorov, N. I. Verbitskiy, D. Haberer, C. Struzzi, L. Petaccia, D. Usachov, O. Y. Vilkov, D. V. Vyalikh, J. Fink, M. Knupfer, B. Büchner, and A. Grüneis, Nature Communications **5**, 3257 (2014).
[63] D. Haberer, L. Petaccia, A. V. Fedorov, C. S. Praveen, S. Fabris, S. Piccinin, O. Vilkov, D. V. Vyalikh, A. Preobrajenski, N. I. Verbitskiy, H. Shiozawa, J. Fink, M. Knupfer, B. Büchner, and A. Grüneis, Physical Review B - Condensed Matter and Materials Physics **88**, 081401(R) (2013).
[64] S. Ichinokura, M. Toyoda, M. Hashizume, K. Horii, S. Kusaka, S. Ideta, K. Tanaka, R. Shimizu, T. Hito-

sugi, S. Saito, and T. Hirahara, Phys. Rev. B **105**, 235307 (2022).
[65] P. Rosenzweig, H. Karakachian, D. Marchenko, K. Küster, and U. Starke, Phys. Rev. Lett. **125**, 176403 (2020).
[66] J. M. Riley, F. Caruso, C. Verdi, L. B. Duffi, M. D. Watson, L. Bawden, K. Volckaert, G. van der Laan, T. Hesjedal, M. Hoesch, F. Giustino, and P. D. C. King, Nature Communications **9**, 2305 (2018).
[67] A. G. Rybkin, A. V. Tarasov, A. A. Rybkina, D. Y. Usachov, A. E. Petukhov, A. V. Eryzhenkov, D. A. Pudikov, A. A. Gogina, I. I. Klimovskikh, G. Di Santo, L. Petaccia, A. Varykhalov, and A. M. Shikin, Phys. Rev. Lett. **129**, 226401 (2022).
[68] Z. Zanolli, C. Niu, G. Bihlmayer, Y. Mokrousov, P. Mavropoulos, M. J. Verstraete, and S. Blügel, Phys. Rev. B **98**, 155404 (2018).
[69] J. Qiao, J. Zhou, Z. Yuan, and W. Zhao, Phys. Rev. B **98**, 214402 (2018).
[70] N. Rougemaille, A. Ndiaye, J. Coraux, C. Vo-Van, O. Fruchart, and A. Schmid, Applied Physics Letters **101**, 142403 (2012).
[71] Z. Qiao, S. A. Yang, W. Feng, W.-K. Tse, J. Ding, Y. Yao, J. Wang, and Q. Niu, Phys. Rev. B **82**, 161414(R) (2010).
[72] Y. Han, Z. Yan, Z. Li, X. Xu, Z. Zhang, Q. Niu, and Z. Qiao, Phys. Rev. B **107**, 205412 (2023).